Journal of Nuclear Medicine, published on September 2, 2022 as doi:10.2967/jnumed.122.264544

PET imaging of fibroblast activation protein in various types of cancers by using ^{68}Ga-FAP-2286: Comparison with ^{18}F-FDG and ^{68}Ga-FAPI-46 in a single-center, prospective study

Running title: ^{68}Ga-FAP-2286 in various cancers

Yizhen Pang[1,2*], Liang Zhao[1,2*], Tinghua Meng[1*], Weizhi Xu[1], Qin Lin[2], Hua Wu[1], Jingjing Zhang[3,5], Xiaoyuan Chen[4,5,6†], Long Sun[1†], and Haojun Chen[1†]

[1] Department of Nuclear Medicine & Minnan PET Center, The First Affiliated Hospital of Xiamen University, Xiamen, China

[2] Department of Radiation Oncology, The First Affiliated Hospital of Xiamen University, Xiamen, China

[3] Department of Diagnostic Radiology, National University of Singapore, Singapore, Singapore

[4] Departments of Diagnostic Radiology, Surgery, Chemical and Biomolecular Engineering, and Biomedical Engineering, Yong Loo Lin School of Medicine and Faculty of Engineering, National University of Singapore, Singapore

[5] Clinical Imaging Research Centre, Centre for Translational Medicine, Yong Loo

Lin School of Medicine, National University of Singapore

[6] Nanomedicine Translational Research Program, NUS Center for Nanomedicine, Yong Loo Lin School of Medicine, National University of Singapore

[†] Corresponding authors

Haojun Chen, MD, PhD

Department of Nuclear Medicine & Minnan PET Center, The First Affiliated Hospital of Xiamen University, Xiamen, China

Tel: +86-592-2137077

Email: leochen0821@foxmail.com

ORCID ID: 0000-0002-9101-8884

Long Sun, MD, PhD

Department of Nuclear Medicine & Minnan PET Center, The First Affiliated Hospital of Xiamen University, Xiamen, China

Email: 13178352662@163.com

Xiaoyuan Chen, PhD

Yong Loo Lin School of Medicine and Faculty of Engineering, National University

of Singapore, Singapore

Email: chen.shawn@nus.edu.sg

Word count: 6190

*** First authors, contributed equally to this work**

Yizhen Pang, Email: pyz15980890201@163.com

Liang Zhao, Email: wzhaoliang01@163.com

Tinghua Meng, Email: 875947209@qq.com

Funding: This work was funded by National Natural Science Foundation of China (82071961), Key Scientific Research Program for Yong Scholars in Fujian (2021ZQNZD016), Fujian Natural Science Foundation for Distinguished Yong Scholars (2022D005), Key Medical and Health Projects in Xiamen (3502Z20209002), and National University of Singapore Start-up Grant (NUHSRO/2020/133/Startup/08, NUHSRO/2021/097/Startup/13).

ABSTRACT

PET imaging targeting fibroblast activation protein (FAP) on the surface of cancer-associated fibroblasts has yielded promising tumor diagnostic results. FAP-2286 contains cyclic peptides as FAP-binding motifs to optimize tumor retention compared with the small molecule FAP inhibitor (FAPI) series (FAPI-04/46). The aim of this study was to evaluate the diagnostic accuracy of the ^{68}Ga-FAP-2286 to detect the primary and metastatic lesions in patients with various types of cancer, compared with ^{18}F-fluorodeoxyglucose (FDG) and ^{68}Ga-FAP-2286. **Methods:** Sixty four patients with 15 types of cancer underwent ^{68}Ga-FAP-2286 PET/ CT for initial assessment or recurrence detection. For comparative purposes, 63 patients underwent paired ^{68}Ga-FAP-2286 and ^{18}F-FDG PET/CT, and 19 patients underwent paired ^{68}Ga-FAP-2286 and ^{68}Ga-FAPI-46 PET/CT imaging. Lesion uptake was quantified as the maximum standardized uptake value (SUVmax) and tumor-to-background ratio. The Wilcoxon matched-pairs signed-rank test was used to compare SUVmax values, and McNemar's test was used to compare the lesion detectability between PET modalities. **Results:** The uptake of ^{68}Ga-FAP-2286 was significantly higher than that of ^{18}F-FDG in primary tumors (median SUVmax: 11.1 *vs.* 6.9, $P < 0.001$), lymph node metastases (median SUVmax: 10.6 *vs.* 6.2, $P < 0.001$), and distant metastases,

resulted in improved image contrast and higher lesion detectability. All primary tumors (46/46) were clearly visualized by ^{68}Ga-FAP-2286 PET/CT, whereas 9 of the 46 lesions could not be visualized via ^{18}F-FDG PET/CT. The lesion detection rate of ^{68}Ga-FAP-2286 PET/CT was superior to that of ^{18}F-FDG PET/CT for involved lymph nodes (98 % [105/107] *vs.* 85 % [91/107], P = 0.001), bone and visceral metastases (95 % [162/171] *vs*. 67 % [114/171], P < 0.001). ^{68}Ga-FAP-2286 yielded similar tumor uptake and lesion detection rates as compared with ^{68}Ga-FAPI-46 in a subcohort of 19 patients. **Conclusion:** ^{68}Ga-FAP-2286 is a promising FAP-inhibitor derivative for safe cancer diagnosis, staging, and restaging. It may be a better alternative to ^{18}F-FDG for the cancer types that exhibit low-to-moderate uptake of ^{18}F-FDG, which including gastric, pancreatic, and liver cancers. In addition, ^{68}Ga-FAP-2286 and ^{68}Ga-FAPI-46 yielded comparable clinical results.

Keywords: fibroblast activation protein; FAP-2286; FAPI-46; PET/CT.

INTRODUCTION

Fluorine-18 fluorodeoxyglucose (^{18}F-FDG), a glucose analog, is extensively used for tumor metabolic imaging. Cancer-associated fibroblasts, one of the most abundant components of the tumor stroma, are alternative targets for the imaging of solid tumors (*1*). Considering the high expression of fibroblast activation protein (FAP) on the cell surfaces of activated cancer-associated fibroblasts and its limited expression in normal tissue, PET imaging of cancer-associated fibroblasts with radiolabeled FAP inhibitors (FAPIs) is a very active field in nuclear medicine (*2*).

^{68}Ga/^{18}F-radiolabeled FAPI variants (including FAPI-04, FAPI-46, and FAPI-74) have yielded promising results in the diagnosis of various cancers (*3-5*). Furthermore, FAPI has been reported to be superior to ^{18}F-FDG in PET/CT imaging of, e.g., liver, gastric, and pancreatic cancer, as well as peritoneal carcinomatosis (*6-9*). However, these FAPI molecules are normally retained in tumors for a relatively short period of time, which may limit their use for radionuclide therapy (*10,11*).

FAP-2286 is a low molecular weight, FAP-targeted polypeptide linked to the chelator, DOTA, which allows for the attachment of radionuclides for imaging and therapeutic use. FAP-2286, developed by using a cyclic peptide as binding motif,

is reportedly to be potent, highly selective for FAP, and stable in human plasma (*12*). In addition, it has a long retention time in tumors, which translates to the robust antitumor efficacy of ^{177}Lu-FAP-2286, as demonstrated in a preclinical study (*12*). In this study, FAP-2286 had a comparable half-maximal effective concentration (4.9 *vs.* 1.7 nM), better cellular internalization, longer retention time, and higher uptake PET/CT scans at all time points in human-embryonic-kidney-FAP cells than FAPI-46. Moreover, ^{177}Lu-FAP-2286 had a significantly higher tumor retention than ^{177}Lu-FAPI-46 at 24 and 72 h after injection, resulting in excellent antitumor efficacy in human-embryonic-kidney-FAP xenografts. The results of a recent pilot study in which ^{177}Lu-FAP-2286 was used for peptide-targeted radionuclide therapy in patients with diverse advanced adenocarcinomas exhibited acceptable side effects and prolonged retention and activity (*13*). The preliminary results from the LuMIERE trial (NCT04939610) reported that ^{177}Lu-FAP-2286 demonstrated a manageable safety profile with some promising efficacy in nine patients with seven types of cancer (partial response was observed in 1 patient who completed 6 cycles of ^{177}Lu-FAP-2286 in 3.7 GBq dose cohort) (*14*). Taken together, FAP-2286 exhibits promising characteristics as a targeting vector with potent and selective FAP binding that leads to intense tumor accumulation and substantial therapeutic efficacy.

In this study, we aimed to investigate the diagnostic accuracy of the novel imaging agent ^{68}Ga-FAP-2286 for detecting the primary and metastatic lesions in patients with various types of cancers, and compared the results with those of ^{18}F-FDG and ^{68}Ga-FAPI-46.

MATERIALS AND METHODS

Participant enrollment

This is a preliminary report of an ongoing, single-center, prospective study of the diagnostic accuracy of ^{68}Ga-FAP-2286 for PET/CT imaging of solid tumors. The institutional review board (IRB 2022KY013) approved this study, and all subjects signed a written informed consent. This study was registered at ClinicalTrials.gov (NCT05392205). The inclusion criteria were as follows: (i) adult participants (aged 18 years or older), (ii) patients with newly diagnosed or previously treated malignant tumors (to avoid the treatment impact on radiotracer uptake, the time interval between the completion of therapy and PET scan was > 6 months), and (iii) patients who were able to provide informed consent or assent according to the guidelines of the Clinical Research Ethics Committee. Exclusion criteria were as follows: (i) patients with nonmalignant disease, (ii) patients who were pregnant, and (iii) research participants, their parents, or their legal

representatives who were unable or unwilling to provide written informed consent.

Radiolabeling

FAP-2286 and FAPI-46 were obtained from Yantai Dongcheng Pharmaceutical Group Co., Ltd. (Shandong, China) and Jiangsu Huayi Technology Co., Ltd. (Jiangsu, China), respectively. Both compounds were used for research purposes. ^{18}F-FDG was manufactured according to the standard method of our laboratory (*15,16*) by using the coincidence ^{18}F-FDG synthesis module (TracerLab FxFN, GE Healthcare, Chicago, IL, USA). The FAPI-46 ligands were radiolabeled with ^{68}Ga according to a previous protocol (*17*). Briefly, 925-1110 MBq $^{68}GaCl_3$ eluted from the ^{68}Ge/^{68}Ga generator (ITG, Germany) was reacted with 25 μg (28.2 nmol) FAPI-46 in 1 mL of 0.25M sodium acetate buffer for 10 min at 100 °C and purified before use. FAP-2286 ligands were radiolabeled with ^{68}Ga in a similar protocol (925-1110 MBq $^{68}GaCl_3$ reacted with 25 μg [17.0 nmol] FAP-2286). Details of the synthesis of radiopharmaceutical are presented in supplemental materials.

PET/CT imaging and evaluation

The dose of intravenously injected ^{68}Ga-FAP-2286 was calculated according to the participants' body weight (1.8–2.2 MBq/kg). At 1 h after intravenous administration, the participants underwent PET/CT imaging via a hybrid PET/CT scanner (Discovery MI, GE Healthcare). All obtained data were transferred to the Advantage Workstation (version AW 4.7, GE Healthcare) and reconstructed using the Bayesian penalized likelihood reconstruction algorithm (Q.clear, GE Healthcare). For patients with malignant disease, additional ^{18}F-FDG and/or ^{68}Ga-FAPI-46 PET/CT scans were performed for comparative purposes, depending on their willingness. The PET/CT imaging protocols for ^{18}F-FDG and ^{68}Ga-FAPI-46 were the same as those for ^{68}Ga-FAP-2286, except that 6 h of fasting was required before the ^{18}F-FDG PET/CT scan (see Supplemental Materials for details) (*18*).

All PET images were evaluated by two board-certified nuclear medicine physicians (C.H. and S.L.), each with at least 10 years of experience in PET/CT imaging; the two physicians were not blinded to the study. Disagreements in opinion were resolved via discussion and consensus. In addition to visual evaluation, lesions were evaluated semiquantitatively by selecting regions of interest. The maximum standardized uptake value (SUVmax) was calculated

automatically by using the A.W. workstation (Version 4.7, GE Healthcare). Regions with radiotracer uptake higher than the background activity in primary tumors, lymph nodes, the lungs, the liver, peritoneal surfaces, and other body parts were considered pathological. Tracer uptakes in normal organs (background) were quantified based on the SUVmean, which was delineated with a diameter of 1 cm (for the small organs, including thyroid, salivary gland, pancreas) to 2 cm (for the other organs, including brain, heart, liver, kidney, spleen, muscle, and bone marrow) sphere placed inside the organ parenchyma. The tumor-to-background ratio (TBR) was calculated as the ratio SUVmax-tumor/SUVmean-background. The physiological uptakes of ^{68}Ga-FAP-2286 and ^{68}Ga-FAPI-46 in normal organs were determined by calculating the SUVmean of background measurements in the heart, liver, spleen, lungs, kidneys, muscles, prostate (men), and uterus (women). Histopathological results obtained via surgery/biopsy served as the gold standard for the final diagnosis. If tissue-based diagnosis was not possible, comprehensive evaluations of multimodal imaging characteristics were used as the reference standard.

Statistical analysis

All statistical analyses were conducted using SPSS 22.0 (IBM, Armonk, NY, USA). The Wilcoxon matched-pairs signed-rank test was used to compare SUVs derived from ^{68}Ga-FAP-2286, ^{68}Ga-FAPI-46, and ^{18}F-FDG PET/CT images. McNemar's test was used to compare the lesion detectability of different PET scans. The paired sample t-test was used to evaluate the differences of normal organs' uptakes between ^{68}Ga-FAP-2286 and ^{68}Ga-FAPI-46 PET/CT. Statistical significance was defined as $P < 0.05$.

RESULTS

Patient characteristics

From March 1st, 2022 to May 31st, 2022, 64 patients with malignant disease (38 men; median age, 57.5 years; range, 32–85 years) who underwent ^{68}Ga-FAP-2286 PET/CT imaging were enrolled in this prospective study (TABLE 1). Among the 64 patients, 44 patients (nine types of cancer) underwent PET/CT imaging for initial assessment (lesion detection and staging), and the other 20 patients (nine types of cancer) underwent PET/CT imaging for detection of tumor recurrence and metastases (restaging). The final diagnosis was based on histopathological results (n = 58) and diagnostic radiology (comprehensive considerations of

imaging findings, n = 6). For comparative purposes, 63 patients underwent paired ^{68}Ga-FAP-2286 and ^{18}F-FDG PET/CT, and 19 patients underwent paired ^{68}Ga-FAP-2286 and ^{68}Ga-FAPI-46 PET/CT. Representative PET images of the three types of PET scans are shown in FIGURE 1.

Adverse events and biodistribution

All patients tolerated the ^{68}Ga-FAP-2286 PET/CT scans. There were no signs of any drug-related pharmacologic effects or other adverse physiological responses. All observed vital signs (including temperature, blood pressure, and heart rate) were normal at the 4 h follow-up. No abnormal symptoms were reported by the patients.

The *in vivo* distribution pattern of ^{68}Ga-FAP-2286 was evaluated and compared with that of ^{68}Ga-FAPI-46 in 19 patients who underwent both scans. ^{68}Ga-FAP-2286 exhibited a similar *in vivo* distribution pattern to that of ^{68}Ga-FAPI-46, except for a slightly higher physiological uptake in the liver and kidneys (FIGURE 2). Semiquantitative analysis demonstrated that ^{68}Ga-FAP-2286 uptakes in the kidneys (5.3 ± 1.5 vs. 2.3 ± 1.2, $t = 8.959$, $P < 0.001$), liver (2.8 ± 1.0 vs. 1.5 ± 0.9, $t = 8.582$, $P < 0.001$), and heart (1.9 ± 0.4 vs. 1.4 ± 0.3, $t = 6.557$, $P < 0.001$) were higher than those of ^{68}Ga-FAPI-46. In contrast, the

background uptakes of ^{68}Ga-FAP-2286 in the thyroid (1.6 ± 0.5 vs. 1.9 ± 0.5, t = -3.537, P = 0.01), pancreas (1.8 ± 0.3 vs. 2.1 ± 0.5, t = -2.559, P = 0.038), muscles (1.3 ± 0.5 vs. 1.5 ± 0.5, t = -2.515, P = 0.04), and salivary glands (2.5 ± 0.6 vs. 3.6 ± 1.0, t = -3.356, P = 0.012) were lower than those of ^{68}Ga-FAPI-46 (FIGURE 2).

^{68}Ga-FAP-2286 and ^{18}F-FDG uptake in cancer patients

Among the 44 patients who underwent paired ^{68}Ga-FAP-2286 and ^{18}F-FDG PET/CT imaging for initial diagnosis, one was diagnosed with a synchronous double cancer (esophageal cancer and lung adenocarcinoma) and one was diagnosed with multifocal breast cancer (four primary tumors in the same breast). In addition, the primary tumors could not be located in two patients with head and neck cancers of unknown primary. Thus, a total of 46 primary tumor lesions (all confirmed by histopathology) were evaluated in this study (TABLE 2). All primary tumors were clearly visualized with intense radiotracer uptake upon ^{68}Ga-FAP-2286 PET/CT imaging, whereas 9 of the 46 lesions could not be visualized via ^{18}F-FDG PET/CT imaging. Primary tumor lesions exhibiting no pathological uptake on ^{18}F-FDG PET/CT images were gastric cancer (n = 3), liver cancer (n = 3), breast cancer (n = 2), and pancreatic cancer (n = 1) (Supplemental Fig. 1). The SUVmax of all primary tumor lesions derived from ^{68}Ga-FAP-2286 PET/CT

imaging was significantly higher than that derived from ^{18}F-FDG PET/CT imaging (11.1 vs. 6.9, $P < 0.001$). Moreover, lesions exhibited a three-fold higher TBR on ^{68}Ga-FAP-2286 PET/CT images than they did on ^{18}F-FDG PET/CT images (9.2 vs. 3.0, $P < 0.001$), thus improving the image contrast for tumor detection and delineation. Representative images are shown in Supplemental Fig. 2.

We investigated the tumor uptake over time by performing ^{68}Ga-FAP-2286 PET scans at multiple time points (0.5, 1, and 3 h after injection) in patients #33 and #54. The SUVmax in patient #33 (nasopharyngeal carcinoma with lymph node and bone metastases) increased by 72.1 % from 0.5 to 3 h in the primary tumor (from 8.6 to 14.8), involved lymph nodes (5.2–69.1 % increase), and one bone metastasis (64.4 % increase) (FIGURE 3). Similar results were observed in patient #54 (metastatic colon cancer); the liver metastases demonstrated a stable ^{68}Ga-FAP-2286 uptake but an increased TBR from 1 to 3 h (Supplemental Fig. 3).

Among the 19 patients who underwent paired ^{68}Ga-FAP-2286 and ^{18}F-FDG PET/CT imaging for cancer restaging, ^{68}Ga-FAP-2286 demonstrated significantly higher lesion detection rates than ^{18}F-FDG PET/CT (100 % [9/9] vs. 33 % [3/9], $P = 0.031$) in nine locally recurrent tumors (all confirmed by histopathology) (Supplemental Fig. 2B). Among all 63 patients who underwent paired ^{68}Ga-FAP-

2286 and ^{18}F-FDG PET/CT imaging for initial staging or restaging, 107 lymph node metastases and 171 bone and visceral metastases were evaluated. Among these, a total of 66 metastatic lesions (12 lymph nodes and 54 bone and visceral metastases) were confirmed by histopathology, and 212 lesions (95 lymph nodes and 117 bone and visceral metastases) were confirmed by diagnostic radiology. ^{68}Ga-FAP-2286 yielded significantly higher radiotracer uptake (SUVmax: 10.6 *vs.* 6.2, $P < 0.001$) and TBR (9.0 *vs.* 3.7, $P < 0.001$) than did ^{18}F-FDG in the metastatic lymph nodes. Therefore, ^{68}Ga-FAP-2286 PET/CT had significantly higher detection rate (98 % [105/107] *vs.* 85 % [91/107], $P = 0.001$) than ^{18}F-FDG PET/CT in the diagnosis of lymph node metastases. Interestingly, the ^{18}F-FDG uptake was positive and ^{68}Ga-FAP-2286 uptake was negative in the enlarged mediastinal lymph nodes in one patient with gastric cancer; these lymph nodes were confirmed to be inflammatory as demonstrated by endobronchial ultrasound-guided transbronchial needle aspiration (Supplemental Fig. 2C). Regarding PET/CT imaging of bone and visceral metastases, ^{68}Ga-FAP-2286 yielded a greater number of positive lesions (95 % [162/171] *vs*. 67 % [114/171], $P < 0.001$) and a higher radiotracer uptake and TBR than ^{18}F-FDG in most of the lesions (liver, peritoneal, subcutaneous, and bone metastases). Interestingly, no significant difference was observed in the SUVmax in liver metastases between

^{68}Ga-FAP-2286 and ^{18}F-FDG, even though the TBR yielded by ^{68}Ga-FAP-2286 (4.1) was twice that yielded by ^{18}F-FDG in those lesions (2.2, $P < 0.001$).

With the new lymph node and visceral metastases detected by ^{68}Ga-FAP-2286 PET/CT, TNM staging was upgraded in 3 patients (3/44, 7%), including one gastric cancer (from IIA to IIB), one esophageal cancer (from IIIA to IIIB), and one nasopharyngeal cancer (from IVA to IVB). Compared to ^{18}F-FDG, ^{68}Ga-FAP-2286 PET/CT detected a greater number of metastatic lesions and/or larger disease extent in 12 patients (12/44, 27%), including pancreatic cancer (n=4), liver cancer (n=2), nasopharyngeal cancer (n=2), esophageal cancer (n=1), ovarian cancer (n=2), and gastric cancer (n=1). Among the other 19 patients in whom recurrence was detected, ^{68}Ga-FAP-2286 PET/CT detected ^{18}F-FDG-negative locally recurrent tumors in six patients (6/19, 32%), and detected ^{18}F-FDG-negative metastatic lesions in seven patients (7/19, 37%). The patients with new lesions and/or larger disease extent detected by ^{68}Ga-FAP-2286 PET/CT are presented in Supplemental Table 1.

^{68}Ga-FAP-2286 and ^{68}Ga-FAPI-46 uptake in patients with cancer

Among the 19 patients who underwent paired ^{68}Ga-FAP-2286 and ^{68}Ga-FAPI-46 PET/CT imaging, 11 patients did so for initial staging and 8 for restaging. The

^{68}Ga-FAP-2286-derived SUVmax was comparable to that derived from ^{68}Ga-FAPI-46 in 13 primary tumor lesions (13.6 *vs.* 13.3, P=0.53; TABLE 3), 4 recurrent tumors (11.2 *vs*. 9.6, P = 0.47), and 33 metastatic lymph nodes (8.3 *vs*. 8.2, P=0.28). Too few patients with each cancer type underwent paired analyses with these modalities to allow for comparisons of radiotracer uptake per tumor type. Regarding visceral and bone metastases, the quantitative tumor uptake of ^{68}Ga-FAP-2286 was not inferior to that of ^{68}Ga-FAPI-46 in the lung (4.0 *vs*. 3.9), liver (4.6 *vs*. 4.4), peritoneal (9.8 *vs*. 11.4), or bone (6.9 *vs*. 5.8) metastases (all P>0.05; TABLE 3). Interestingly, in one patient with metastatic cholangiocarcinoma, the median SUVmax of ^{68}Ga-FAP-2286 was significantly higher than that of ^{68}Ga-FAPI-46 (8.1 vs. 6.0, P=0.022) in the widespread subcutaneous metastases, and ^{68}Ga-FAP-2286 PET/CT detected a greater number of subcutaneous metastases than ^{68}Ga-FAPI-46 (25 *vs.* 16). Representative images are shown in FIGURE 4, FIGURE 5, and FIGURE 6, respectively.

DISCUSSION

In this study, we conducted clinical investigations using ^{68}Ga-FAP-2286 for PET/CT imaging in patients with different types of cancers. We aimed to

investigate whether ^{68}Ga-FAP-2286 could be used for cancer imaging, and compared it with ^{18}F-FDG and ^{68}Ga-FAPI-46.

The encouraging results from a preclinical study and a first-in-human study (*12,13*) warranted further clinical evaluation of ^{68}Ga-FAP-2286. Therefore, we are in the process of investigating the diagnostic accuracy of ^{68}Ga-FAP-2286 for the identification of FAP-positive solid tumors via PET/CT imaging. First, we evaluated the *in vivo* distribution pattern of ^{68}Ga-FAP-2286 and compared it with that of ^{68}Ga-FAPI-46. The physiological uptake of ^{68}Ga-FAP-2286 was lower than ^{68}Ga-FAPI-46 in the muscles, salivary glands, thyroid, and pancreas. However, ^{68}Ga-FAP-2286 uptake in the kidneys, liver, and heart were higher than that of ^{68}Ga-FAPI-46, thus suggesting that the cyclopeptide structure of FAP-2286 may lead to altered *in vivo* pharmacokinetics. Cyclic peptides may have improved biological properties compared with the small molecule FAPI series (*19*), including stronger receptor selectivity and binding affinity, owing to increased plasma stability and conformational rigidity. Indeed, ^{177}Lu-FAP-2286 had a long effective half-life in the first-in-human study (35 ± 9 h in the entire body and 44 ± 25 h in the bone metastases) (*13*). Moreover, the tumor uptake in our study increased in one patient and remained stable in the other, from 0.5 to 3 h after injection. In preclinical studies, FAP-2286 demonstrated longer tumor retention

than FAPI-46 at later timepoints (*12*), and greater antitumor efficacy was observed in tumor xenografts with ^{177}Lu-FAP-2286 than with ^{177}Lu-FAPI-46. Taken together, an increased FAP-binding affinity, improved tumor accumulation, and longer tumor retention are the main potential advantages of FAP-2286 compared with other FAPI variants. In our study, the results from PET imaging demonstrated that tumor uptake of ^{68}Ga-FAPI-46 and ^{68}Ga-FAP-2286 were comparable at earlier timepoints, thus indicating that both two compounds can be used for imaging of FAP-positive tumors. Further studies with larger patient population are needed to test the role of ^{68}Ga-FAP-2286 among the existing FAPI derivatives.

Another aim of the present study was to compare the tumor uptake and lesion detectability between ^{68}Ga-FAP-2286 and ^{18}F-FDG PET/CT imaging. With respect to primary tumor lesions, the quantitative tumor uptake and TBR were significantly higher with ^{68}Ga-FAP-2286 than with ^{18}F-FDG. This corresponds to the results which showed that all primary tumors (46/46) were identified with ^{68}Ga-FAP-2286, whereas nine were missed with ^{18}F-FDG (Supplemental Fig. 1). Consistent with previous FAPI-based imaging studies (*7*-*9*), ^{68}Ga-FAP-2286 PET/CT imaging was superior to ^{18}F-FDG PET/CT imaging in gastrointestinal malignancies, including gastric, pancreatic, and liver cancer. This result suggests

that ^{68}Ga-FAP-2286 PET/CT imaging is a promising modality in the diagnosis of these cancer types for which ^{18}F-FDG PET/CT imaging is inadequate. Regarding the detection of lymph node and visceral metastases, ^{68}Ga-FAP-2286 yielded a higher radiotracer uptake and TBR than ^{18}F-FDG, and resulted in improved lesion detectability, particularly of liver, bone, and peritoneal metastases. Interestingly, we noted that one patient (Supplemental Fig. 2C) with reactive lymph nodes did not exhibit increased ^{68}Ga-FAP-2286 uptake, whereas false-positive ^{18}F-FDG uptake was observed in these nodules. Similar findings have been reported in previous studies (*20*). Thus, we speculate that ^{68}Ga-FAP-2286 may be more suitable than ^{18}F-FDG for differentiating reactive lymph nodes from tumor metastatic lymph nodes. However, tumor/inflammation differentiation by ^{68}Ga-FAP-2286 PET/CT was not the main aim of this study, although this question should be investigated in future clinical trials.

Overall, the results from this study suggest that ^{68}Ga-FAP-2286 is a promising FAPI molecule for cancer diagnosis, staging, and restaging. Therefore, ^{68}Ga-FAP-2286 PET/CT may contribute to the diagnosis of solid tumors, especially in malignant tumors with low-to-moderate uptake in ^{18}F-FDG PET/CT. The specific cancer types that showed that ^{68}Ga-FAP-2286 is superior to ^{18}F-FDG include gastric, pancreatic, and liver cancers; respective findings were in

line with previous publications (*7*). Specifically, pancreatic and liver cancers (especially intrahepatic cholangiocarcinoma) are characterized by intense stromal desmoplastic reactions surrounding cancer cells, and CAFs are the main effector cells in the desmoplastic reaction (*21,22*). Furthermore, due to the low background uptake in liver parenchyma, FAP imaging was able to detect liver tumors with favorable tumor-to-background contrast. Gastric cancer evokes the production and deposition of activated fibroblasts in the submucosa wall (*23*), resulting in increased ^{68}Ga-FAPI uptake in gastric tumor lesions. Differ from ^{18}F-FDG, very low ^{68}Ga-FAPI uptake was observed in the gastric wall and gastrointestinal tract, which further improved the lesion detectability of gastric cancer. Taken together, high-FAP expressions and low background activities of abdominal organs are the main reasons and explain why ^{68}Ga-FAP-2286 PET/CT is superior to ^{18}F-FDG in terms of tumor detectability in these tumor entities. Improved tumor detectability may lead to changes in clinical staging and optimization of therapeutic strategies. Moreover, the favorable TBR may improve delineation of gross tumors in radiotherapy and evaluation of the effectiveness of therapy (*24,25*).

Our study was associated with several limitations. First, few patients underwent paired ^{68}Ga-FAP-2286 and ^{18}F-FDG PET/CT imaging, rendering

subgroup analysis of radiotracer uptake per tumor type impracticable. Second, as the subcohort of patients who underwent paired ^{68}Ga-FAP-2286 and ^{68}Ga-FAPI-46 PET/CT imaging was also small (n = 19), this only allowed for descriptive comparison. Furthermore, as only two patients underwent ^{68}Ga-FAP-2286 PET/CT scans at multiple time points, we could not fully investigate radiotracer retention in tumors. Prospective studies with a larger patient population are warranted in the future to better explore the role of ^{68}Ga-FAP-2286 in cancer diagnosis and the potential superiority of FAP-2286 with respect to other FAPI derivatives.

CONCLUSION

^{68}Ga-FAP-2286 is a promising FAPI derivative for safe cancer diagnosis, staging, and restaging. It may be superior to ^{18}F-FDG in selected cases, especially for cancers that exhibit low-to-moderate uptake of ^{18}F-FDG, including gastric, pancreatic, and liver cancers. In addition, ^{68}Ga-FAP-2286 and ^{68}Ga-FAPI-46 yielded comparable clinical results.

Disclosures

Funding: This work was funded by National Natural Science Foundation of China (82071961), Key Scientific Research Program for Yong Scholars in Fujian (2021ZQNZD016), Fujian Natural Science Foundation for Distinguished Yong Scholars (2022D005), Key Medical and Health Projects in Xiamen (3502Z20209002), and National University of Singapore Start-up Grant (NUHSRO/2020/133/Startup/08, NUHSRO/2021/097/Startup/13).

Conflicts of interest: No potential conflicts of interest relevant to this article exist.

KEY POINTS

QUESTION: Is ^{68}Ga-FAP-2286 an efficacious alternative for the imaging of FAP-positive tumors?

PERTINENT FINDINGS: This is a preliminary report of a single-center, prospective study of the diagnostic accuracy of ^{68}Ga-FAP-2286 PET/CT imaging of solid tumors. All 46 primary tumors in nine types of cancer were identified with ^{68}Ga-FAP-2286, whereas nine were missed with ^{18}F-FDG; ^{68}Ga-FAP-2286 yielded a higher radiotracer uptake and TBR than ^{18}F-FDG. In addition, ^{68}Ga-FAP-2286 and ^{68}Ga-FAPI-46 yielded comparable clinical results.

IMPLICATIONS FOR PATIENT CARE: ^{68}Ga-FAP-2286 is a promising FAP-inhibitor derivative for safe cancer diagnosis, staging, and restaging.

References

1. Backhaus P, Gierse F, Burg MC, et al. Translational imaging of the fibroblast activation protein (FAP) using the new ligand [(68)Ga]Ga-OncoFAP-DOTAGA. *Eur J Nucl Med Mol Imaging.* 2022;49:1822-1832.

2. Kratochwil C, Flechsig P, Lindner T, et al. (68)Ga-FAPI PET/CT: Tracer Uptake in 28 Different Kinds of Cancer. *J Nucl Med.* 2019;60:801-805.

3. Li M, Younis MH, Zhang Y, Cai W, Lan X. Clinical summary of fibroblast activation protein inhibitor-based radiopharmaceuticals: cancer and beyond. *Eur J Nucl Med Mol Imaging.* 2022;49:2844-2868.

4. Pang Y, Zhao L, Luo Z, et al. Comparison of (68)Ga-FAPI and (18)F-FDG Uptake in Gastric, Duodenal, and Colorectal Cancers. *Radiology.* 2021;298:393-402.

5. Zhao L, Chen J, Pang Y, et al. Fibroblast activation protein-based theranostics in cancer research: A state-of-the-art review. *Theranostics.* 2022;12:1557-1569.

6. Shi X, Xing H, Yang X, et al. Comparison of PET imaging of activated fibroblasts and (18)F-FDG for diagnosis of primary hepatic tumours: a prospective pilot study. *Eur J Nucl Med Mol Imaging.* 2021;48:1593-1603.

7. Chen H, Pang Y, Wu J, et al. Comparison of [(68)Ga]Ga-DOTA-FAPI-04 and [(18)F] FDG PET/CT for the diagnosis of primary and metastatic lesions in patients with various types of cancer. *Eur J Nucl Med Mol Imaging.* 2020;47:1820-1832.

8. Pang Y, Zhao L, Shang Q, et al. Positron emission tomography and computed tomography with [(68)Ga]Ga-fibroblast activation protein inhibitors improves tumor detection and staging in patients with pancreatic cancer. *Eur J Nucl Med Mol Imaging.* 2022;49:1322-1337.

9. Qin C, Shao F, Gai Y, et al. (68)Ga-DOTA-FAPI-04 PET/MR in the Evaluation of Gastric Carcinomas: Comparison with (18)F-FDG PET/CT. *J Nucl Med.* 2022;63:81-88.

10. Loktev A, Lindner T, Burger EM, et al. Development of Fibroblast Activation Protein-Targeted Radiotracers with Improved Tumor Retention. *J Nucl Med.* 2019;60:1421-1429.

11. Fu K, Pang Y, Zhao L, et al. FAP-targeted radionuclide therapy with [(177)Lu]Lu-FAPI-46 in metastatic nasopharyngeal carcinoma. *Eur J Nucl Med Mol Imaging.* 2022;49:1767-1769.

12. Zboralski D, Hoehne A, Bredenbeck A, et al. Preclinical evaluation of FAP-2286 for fibroblast activation protein targeted radionuclide imaging and therapy. *Eur J Nucl Med Mol Imaging.* May 24,2022 [Epub ahead of print].

13. Baum RP, Schuchardt C, Singh A, et al. Feasibility, Biodistribution, and Preliminary Dosimetry in Peptide-Targeted Radionuclide Therapy of Diverse Adenocarcinomas Using (177)Lu-FAP-2286: First-in-Humans Results. *J Nucl Med.* 2022;63:415-423.

14. McConathy J, Dhawan M, Goenka A, et al. 177Lu-FAP-2286 in patients with advanced or metastatic solid tumors: Initial data from a phase 1/2 study investigating safety, pharmacokinetics, dosimetry, and preliminary antitumor activity (LuMIERE). *Journal of Nuclear Medicine.* 2022;63:2271.

15. Zhao L, Zhuang Y, Fu K, et al. Usefulness of [(18)F]fluorodeoxyglucose PET/CT for evaluating the PD-L1 status in nasopharyngeal carcinoma. *Eur J Nucl Med Mol Imaging.* 2020;47:1065-1074.

16. Yu S. Review of F-FDG Synthesis and Quality Control. *Biomed Imaging Interv J.* 2006;2:e57.

17. Meyer C, Dahlbom M, Lindner T, et al. Radiation Dosimetry and Biodistribution of (68)Ga-FAPI-46 PET Imaging in Cancer Patients. *J Nucl Med.* 2020;61:1171-1177.

18. Boellaard R, Delgado-Bolton R, Oyen WJ, et al. FDG PET/CT: EANM procedure guidelines for tumour imaging: version 2.0. *Eur J Nucl Med Mol Imaging.* 2015;42:328-354.

19. Parker MFL, Blecha J, Rosenberg O, Ohliger M, Flavell RR, Wilson DM. Cyclic (68)Ga-Labeled Peptides for Specific Detection of Human Angiotensin-Converting Enzyme 2. *J Nucl Med.* 2021;62:1631-1637.

20. Zhou X, Wang S, Xu X, et al. Higher accuracy of [(68) Ga]Ga-DOTA-FAPI-04 PET/CT comparing with 2-[(18)F]FDG PET/CT in clinical staging of NSCLC. *Eur J Nucl Med Mol Imaging.* 2022;49:2983-2993.

21. Guo W, Pang Y, Yao L, et al. Imaging fibroblast activation protein in liver cancer: a single-center post hoc retrospective analysis to compare [(68)Ga]Ga-FAPI-04 PET/CT versus MRI and [(18)F]-FDG PET/CT. *Eur J Nucl Med Mol Imaging.* 2021;48:1604-1617.

22. Nielsen MF, Mortensen MB, Detlefsen S. Key players in pancreatic cancer-stroma interaction: Cancer-associated fibroblasts, endothelial and inflammatory cells. *World J Gastroenterol.* 2016;22:2678-2700.

23. Zhang J, Li S, Zhao Y, et al. Cancer-associated fibroblasts promote the migration and invasion of gastric cancer cells via activating IL-17a/JAK2/STAT3 signaling. *Ann Transl Med.* 2020;8:877.

24. Windisch P, Zwahlen DR, Koerber SA, et al. Clinical Results of Fibroblast Activation Protein (FAP) Specific PET and Implications for Radiotherapy Planning: Systematic Review. *Cancers (Basel).* 2020;12:2629.

25. Zhao L, Pang Y, Zheng H, et al. Clinical utility of [(68)Ga]Ga-labeled fibroblast activation protein inhibitor (FAPI) positron emission tomography/computed tomography for primary staging and recurrence detection in nasopharyngeal carcinoma. *Eur J Nucl Med Mol Imaging.* 2021;48:3606-3617.

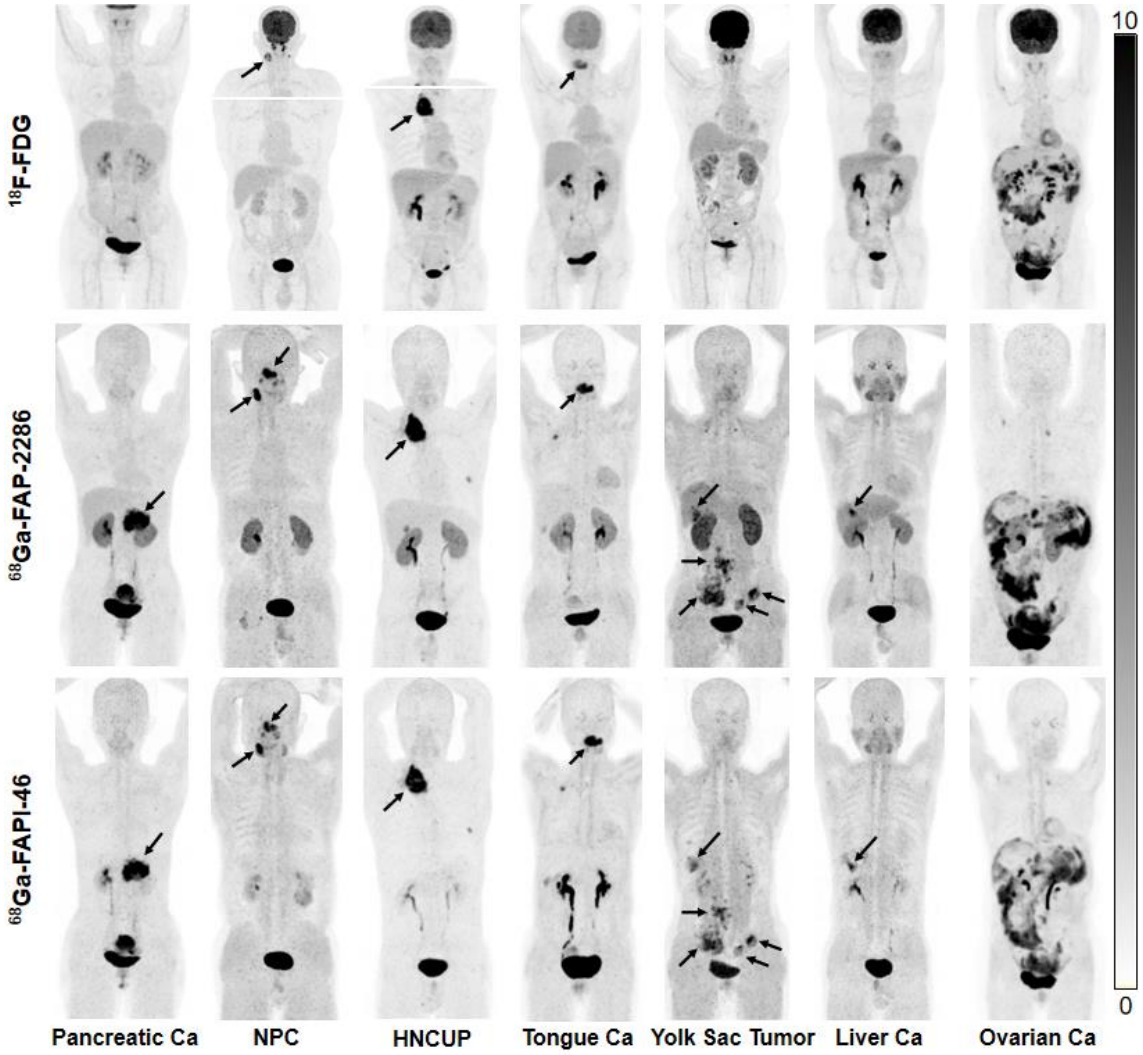

FIGURE 1. Maximum-intensity projection images of ^{18}F-fluorodeoxyglucose (FDG), ^{68}Ga-FAP-2286, and ^{68}Ga-FAPI-46 PET/CT imaging in seven patients with different types of cancer (histologically confirmed). Tumor lesions are indicated with arrows.

Abbreviation: Ca = carcinoma, HNCUP = head and neck carcinoma of unknown primary, NPC = nasopharyngeal carcinoma.

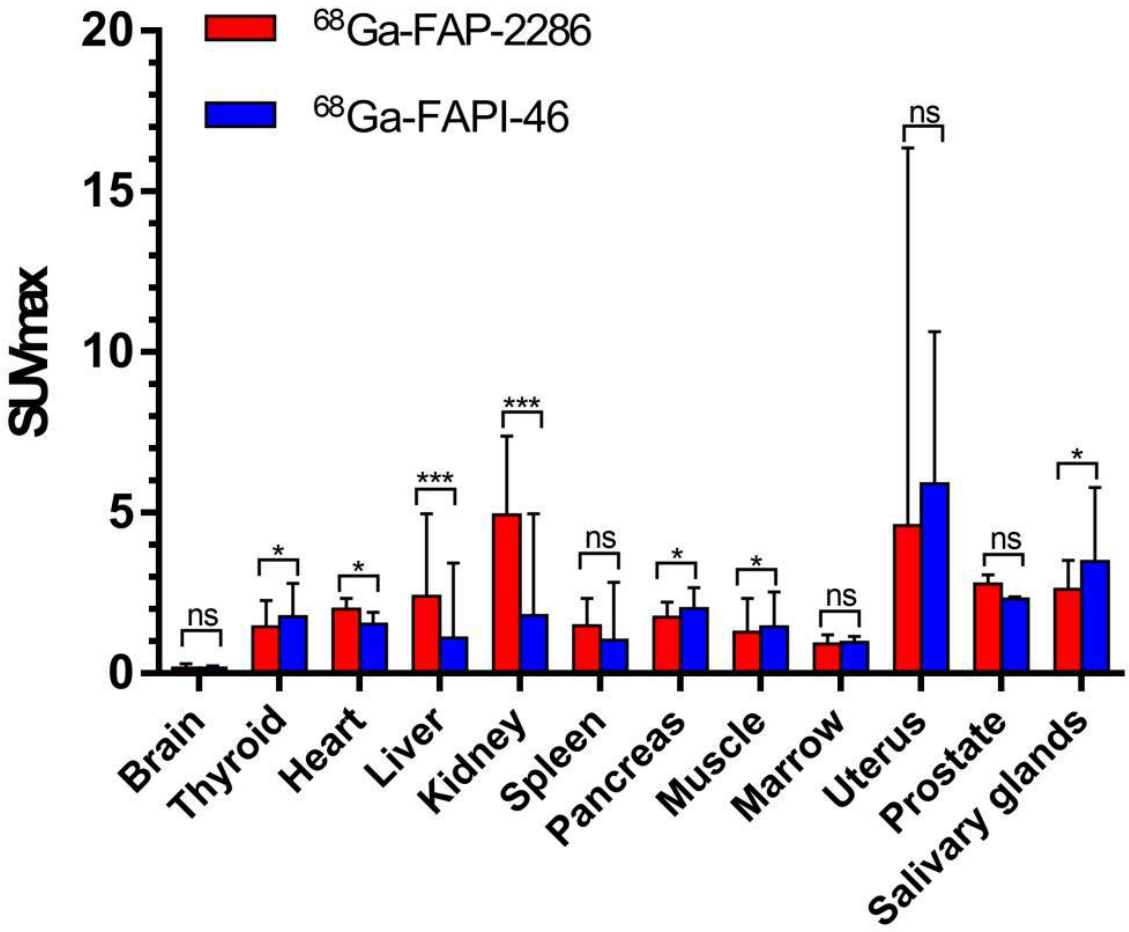

FIGURE 2. PET-based biodistribution analysis of ^{68}Ga-FAP-2286 and ^{68}Ga-FAPI-46 in normal organs at 1 h after injection. Results are shown as the means and standard deviations values from 19 patients.

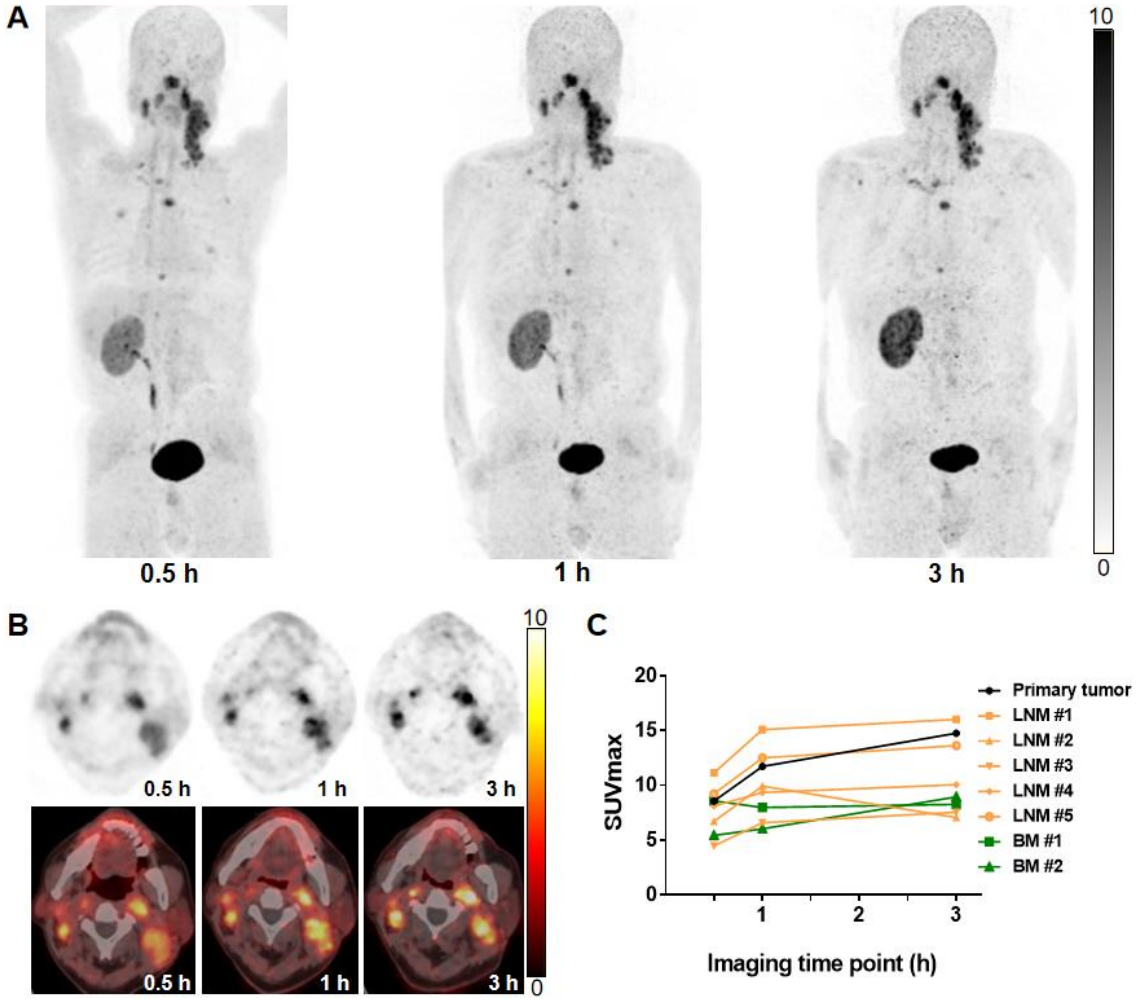

FIGURE 3. A 66-year-old man with nasopharyngeal carcinoma underwent ^{68}Ga-FAP-2286 PET/CT imaging at different time points after injection. Rapid and stable radiotracer uptake was observed in both primary and metastatic lesions. Semiquantitative analysis demonstrated an increase in SUVmax from 0.5 to 3 h in the primary tumor (from 8.6 to 14.8, 72.1 % increase), involved lymph nodes (5.2–69.1 % increase), and one bone metastasis (64.4 % increase).

Abbreviation: BM = bone metastasis, LNM = lymph node metastasis.

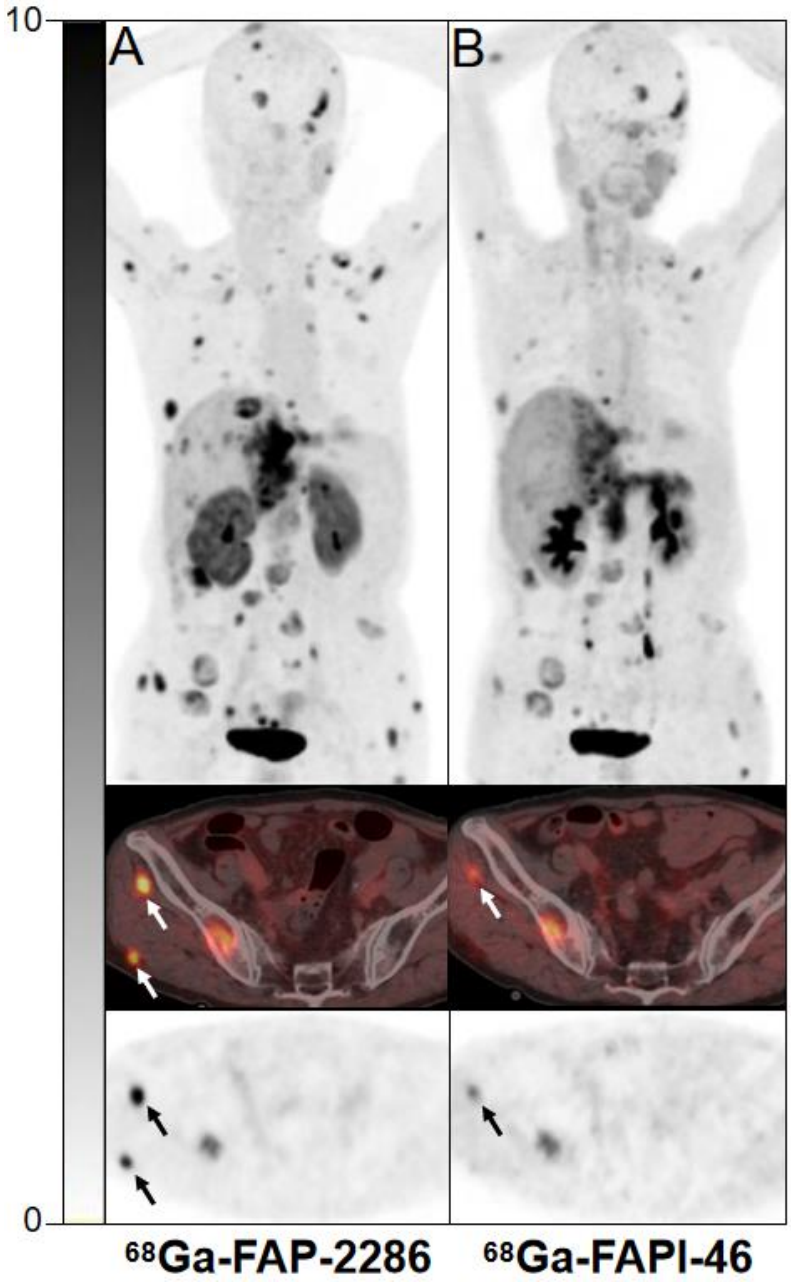

FIGURE 4. A 65-year-old woman with metastatic intrahepatic cholangiocarcinoma underwent imaging for cancer restaging; ^{68}Ga-FAP-2286 (A) revealed a greater number of metastases and higher uptake than ^{68}Ga-FAPI-46 (B) in the widespread subcutaneous metastases (arrows).

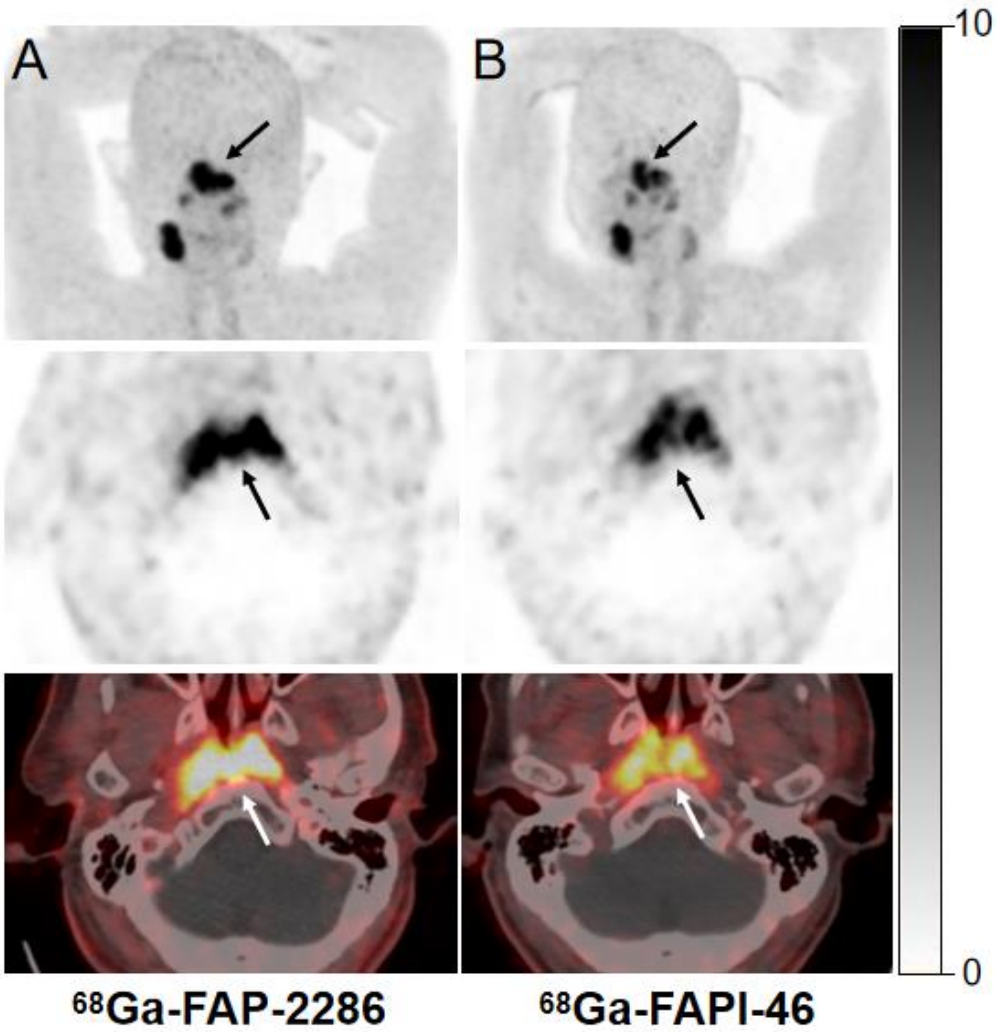

FIGURE 5. A 72-year-old man with newly diagnosed nasopharyngeal carcinoma underwent PET/CT for tumor staging. ^{68}Ga-FAP-2286 PET/CT (A) showed higher radiotracer uptake in the primary tumor (SUVmax, 17.4 *vs.* 12.2, arrows) than ^{68}Ga-FAPI-46 (B).

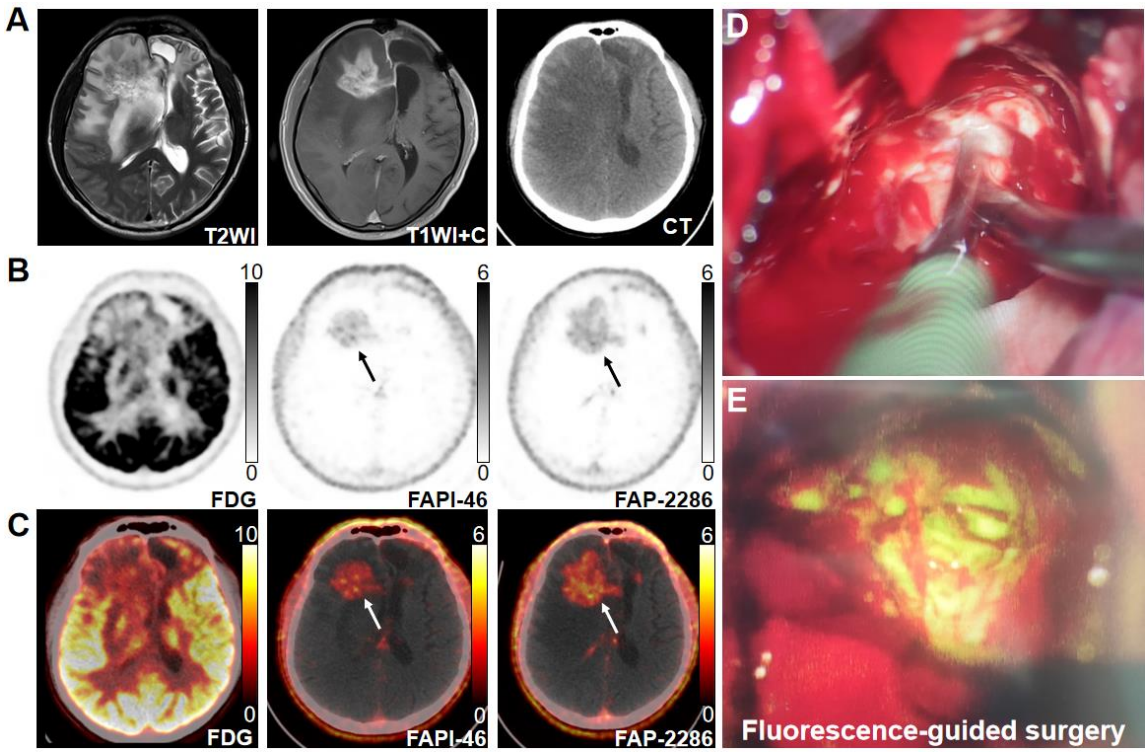

FIGURE 6. A 44-year-old man with glioblastoma underwent surgical resection 1 year before the images were obtained. Magnetic resonance imaging revealed suspicious recurrent lesions in the right frontal lobe adjacent to the surgical margin (arrow) (A). ^{68}Ga-FAP-2286 PET/CT yielded higher radiotracer uptake (SUVmax, 4.2 *vs.* 2.7; arrows) and tumor-to-background ratio (70.0 vs. 45.0) than ^{68}Ga-FAPI-46 in these lesions (B-C). The patient subsequently underwent surgical resection (D-E), and postoperative pathology confirmed the diagnosis of recurrent glioblastoma.

Graphical Abstract

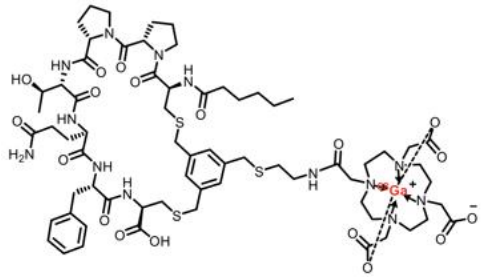

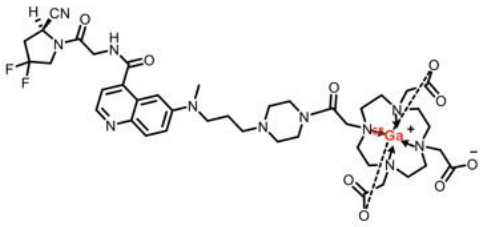

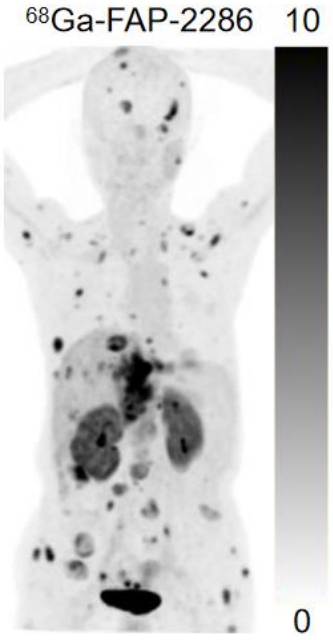

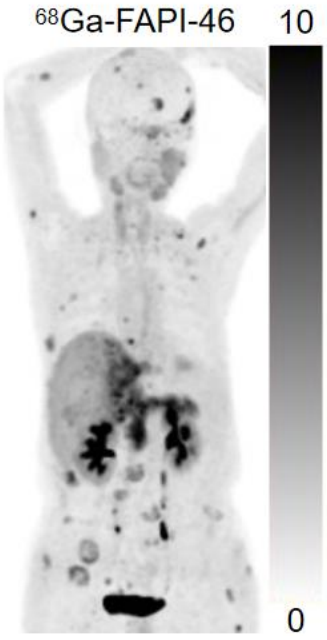

TABLE 1. Patients' characteristics (*n* = 64)

Characteristics	Number
Number of patients	64
Patients with paired ^{68}Ga-FAP-2286 and ^{18}F-FDG PET/CT	63
Time interval between ^{68}Ga-FAP-2286 and ^{18}F-FDG PET/CT	1-7 days
Patients with paired ^{68}Ga-FAP-2286 and ^{68}Ga-FAPI-46 PET/CT	19
Time interval between ^{68}Ga-FAP-2286 and ^{68}Ga-FAPI-46 PET/CT	1-4 days
Age (y)	
Median (range)	57.5 (32–85)
Sex	
Male	38
Female	26
Types of cancer	
Head and neck cancer	15
Liver cancer	12
Gastric cancer	10
Pancreatic cancer	7
Ovarian cancer	5
Esophageal cancer*	4
Breast cancer	3
Non-small cell lung cancer*	2
Renal cancer	2
Glioblastoma	1
Thymic carcinoma	1
Colorectal cancer	1
Yolk sac tumor	1
Gastrointestinal stromal tumor	1
Clinical reason for PET/CT	
Detection of unknown primary tumor	3
Staging of cancer	39
Evaluation of doubtful lesions	2
Identification of disease recurrence	20
Final diagnosis	
Histopathological confirmation (via biopsy or surgery)	58
Diagnostic imaging/follow-up	6

*One patient was diagnosed with synchronous double cancer (esophageal and lung adenocarcinoma).

TABLE 2. Comparison of SUVmax on ^{68}Ga-FAP-2286 and ^{18}F-FDG PET/CT images in primary and metastatic tumors

		Size (cm)	^{68}Ga-FAP-2286			^{18}F-FDG PET/CT			P value	
Primary tumor	n	Median (range)	No. of positive tumors	SUVmax (median, range)	TBR (median, range)	No. of positive tumors	SUVmax (median, range)	TBR (median, range)	Median SUVmax (FAP-2286 vs. FDG)	TBR (FAP-2286 vs. FDG)
Total[§]	46	3.2 (0.9–11.3)	46	11.1 (2.5–28.9)	9.2 (1.1–31.5)	37	6.9 (1.5–19.1)	3.0 (0.9-13.2)	<0.001	<0.001
HNC	7	1.7 (1.5–3.4)	7	16.8 (11.0–20.2)	13.7 (8.1–15.3)	7	11.0 (4.0–15.6)	7.0 (2.9-13.1)	0.043	0.043
Breast cancer*	6	1.5 (0.9–7.0)	6	9.9 (6.0–18.3)	10.1 (3.9–22.3)	4	6.4 (1.5–17.3)	5.0 (1.1-13.2)	0.249	0.075
Esophageal cancer	4	4.1 (2.1–9.0)	4	22.9 (10.0–26.4)	13.6 (6.3–19.4)	4	11.6 (7.9–18.4)	5.8 (4.7-8.6)	0.068	0.068
Lung adenocarcinoma	2	2.9 (1.1–4.7)	2	7.5 (5.7–9.3)	10.0 (9.2–10.9)	2	6.1 (3.3–8.9)	7.1 (4.2-10.0)	NA	NA
Gastric cancer	6	2.0 (1.2–4.5)	6	9.1 (4.1–13.0)	9.2 (4.9–12.7)	3	3.4 (1.7–7.9)	2.0 (0.9-4.1)	0.028	0.028
Liver cancer	8	5.2 (0.9–11.3)	8	11.3 (2.5–28.9)	5.2 (1.5–9.4)	5	4.8 (3.1–9.7)	1.5 (1.0-3.5)	0.917	0.028
Pancreatic cancer	7	3.4 (2.4–5.7)	7	13.0 (10.7–22.7)	12.2 (5.7–23.3)	6	6.5 (3.0–8.1)	2.9 (1.1-4.4)	0.018	0.018
Renal cancer	1	4.5 (NA)	1	6.1 (NA)	1.5 (NA)	1	4.1 (NA)	2.0 (NA)	NA	NA
Ovarian cancer	5	4.8 (1.7–6.2)	5	10.8 (6.0–25.6)	11.0 (5.0–31.5)	5	9.6 (5.3–12.2)	6.9 (2.8-9.3)	0.345	0.138

		Size (cm)	^{68}Ga-FAP-2286 PET/CT			^{18}F-FDG PET/CT			P value	
Recurrence/ metastases	n	Median (range)	No. of positive lesions	SUVmax (median, range)	TBR (median, range)	No. of positive lesions	SUVmax (median, range)	TBR (median, range)	Median SUVmax (FAP-2286 vs. FDG)	TBR (FAP-2286 vs. FDG)
Recurrent tumor (Total[†])	9	2.9 (0.7–5.1)	9	5.8 (2.9–16.5)	4.7 (2.2–15.7)	3	3.8 (2.2–7.6)	1.1 (0.8–5.4)	0.015	0.008
LN mets (Total)	107	1.2 (0.5–6.6)	105	10.6 (3.0–20.1)	9.0 (2.2–30.0)	91	6.2 (1.3–21.2)	3.7 (1.0–13.0)	<0.001	<0.001
Lung mets	21	0.9 (0.4–1.3)	16	3.4 (0.6–10.2)	4.9 (0.9–14.5)	19	3.5 (0.7–7.1)	5.0 (1.0–10.2)	0.876	0.931
Liver mets	30	2.6 (0.9–10.7)	27	6.9 (2.4–12.2)	4.1 (0.9–8.4)	22	6.8 (2.1–10.8)	2.2 (0.9–3.9)	0.484	<0.001
Peritoneal mets	70	NA[‡]	69	8.6 (2.4–15.4)	6.7 (1.8–27.0)	46	4.6 (1.5–11.4)	2.4 (0.8–8.1)	<0.001	<0.001
Subcutaneous mets	12	0.9 (0.6–2.0)	12	8.1 (5.2–12.4)	9.3 (6.3–20.4)	5	1.4 (0.7–7.4)	1.3 (1.0–11.6)	0.002	0.002
Bone mets	38	1.0 (0.4–3.1)	38	6.6 (3.8–13.3)	10.1 (2.9–26.7)	22	2.7 (0.9–11.4)	2.4 (0.9–19.3)	<0.001	<0.001

*One patient was diagnosed with multifocal breast cancer (four primary tumors).

[†]Local recurrent tumors included glioblastoma (n=1), HNC (n = 4), liver cancer (n = 3), and gastric cancer (n = 1).

[‡]Lesion size cannot be calculated owing to the diffuse type of peritoneal metastases (irregular shape).

[§]Primary tumors were not located in two patients with head and neck cancer of unknown primary etiology; the two patients were therefore excluded from the analysis. Two patients were diagnosed with synchronous double cancer (one with esophageal and lung adenocarcinoma, the other with HNC and renal cancer).

Abbreviation: HNC = head and neck cancer, mets = metastases, LN = lymph node, TBR = tumor-to-background ratio, NA = not applicable.

TABLE 3. Comparison of SUVmax on FAP-2286 and FAPI-46 PET/CT images in primary and metastatic lesions

Primary tumors	n	Tumor size (cm)	Tracer	SUVmax (median, range)		P value
Total*	13	3.6 (1.0–6.2)	FAP-2286	13.6 (2.5–25.8)		0.53
			FAPI-46	13.3 (2.4–21.8)		
Recurrence/ metastases	**n**	**Tumor size (cm)**	**Tracer**	**No. of positive lesions**	**SUVmax, (median, range)**	**P value**
Recurrent tumor (total)†	4	3.1 (2.6–5.1)	FAP-2286	4	11.2 (2.7–14.4)	0.465
			FAPI-46	4	9.6 (2.9–13.6)	
Lymph node mets (total)	33	1.2 (0.6–4.6)	FAP-2286	35	8.3 (3.4–15.6)	0.28
			FAPI-46	35	8.2 (4.0–15.4)	
Lung mets	2	0.9 (0.8–1.0)	FAP-2286	2	4.0 (3.8–4.2)	NA
			FAPI-46	2	3.9 (3.6–4.2)	
Liver mets	6	2.0 (0.9–11.8)	FAP-2286	6	4.6 (2.7–7.2)	0.345
			FAPI-46	6	4.4 (2.9–8.5)	
Subcutaneous mets	10	0.8 (0.6–2.0)	FAP-2286	10	8.1 (7.4–10.3)	0.022
			FAPI-46	10	6.0 (3.6–8.6)	
Peritoneal mets	22	NA‡	FAP-2286	22	9.8 (6–15.4)	0.18
			FAPI-46	22	11.4 (7.4–19.2)	
Bone mets	10	1.3 (0.7–2.5)	FAP-2286	10	6.9 (3.9–12.2)	0.074
			FAPI-46	10	5.8 (2.9–11.4)	

*Primary tumors included head and neck Ca (n = 2), esophageal Ca (n = 1), lung adenocarcinoma (n=1), liver Ca (n = 2), gastric Ca (n = 1), pancreatic Ca (n = 4), renal Ca (n = 1), and ovarian Ca (n = 1)

†Including glioblastoma, tongue cancer, liver cancer, and gastric cancer.

‡Peritoneal mets were statistically analyzed according to the peritoneal cancer index score, so the size of the lesions could not be obtained.

Abbreviation: Ca = cancer, mets = metastases, NA = not applicable.

Supplemental materials

Radiochemical Processing

^{18}F-FDG was synthesized in-house by a cyclotron (MINItrace, GE Healthcare) in accordance with the standard methods, using the coincidence ^{18}F-FDG synthesis module (TracerLab FxFN, GE Healthcare) (*16*). The precursor FAP-2286 and FAPI-46 were obtained from Yantai Dongcheng Pharmaceutical Group Co., Ltd (Shandong, China) and Jiangsu Huayi Technology Co., Ltd. (Jiangsu, China), respectively. Both compounds were used for research purpose. Radiolabeling of ^{68}Ga-FAPI-46 was performed according to previously described protocols (*17*). $^{68}Ga^{3}$+ was eluted from ^{68}Ge/^{68}Ga generator (ITG, Germany). The elution volume of $^{68}Ga^{3+}$ (925-1110 MBq in 0.6M HCl, 4 ml) was added to a solution of FAPI-46 (25 μg [28.2 nmol] in sodium acetate, 1mL). The reactor vial was heated to 100℃ for 10 min. After trapping of on a solid-phase cartridge (Sep-Pak C18 Plus Light Cartridge, Waters, USA), the cartridge was washed with water (20mL). The elution of ^{68}Ga-FAPI-46 was performed by using 75% ethanol (1.0 ml) and the final formulation of ^{68}Ga-FAPI-46 was diluted with normal saline (14 mL). The radiolabeling of ^{68}Ga-FAP-2286 was performed in a similar protocol, with a reaction mixture of 25 μg (17.0 nmol) FAP-2286 and 925-1110 MBq ^{68}Ga solution. Quality control of the radiosynthesis was performed by ultraviolet and radio-high performance liquid chromatography (HPLC). The radiochemical purity was over 95% for both ^{68}Ga-FAP-2286 and ^{68}Ga-FAPI-46,

and the final product was diluted with saline and sterilised by passing through a 0.22-μm Millipore filter into a sterile multidose syringe. The final product was sterile and pyrogen-free.

PET/CT imaging and reconstruction

^{18}F-FDG PET/CT was performed within 7 days of ^{68}Ga-FAP-2286 PET/CT scan. Patients were instructed to fast for at least 6 h before ^{18}F-FDG PET/CT scan and to drink 500 mL of water before the scan to stimulate ^{18}F-FDG excretion from the renal calyces and subsequent voiding (*18*). A normal blood glucose level in the peripheral blood was ensured on ^{18}F-FDG PET/CT imaging evaluation. In a certain group of patients, ^{68}Ga-FAPI-46 PET/CT was performed within 7 days of ^{68}Ga-FAP-2286 PET/CT for a direct comparison between the two FAPI derivatives. No specific preparation was required before ^{68}Ga-FAPI-2286 and ^{68}Ga-FAPI-46 PET/CT scans.

The injected activities for ^{18}F-FDG were 288.1±28.4 MBq (range, 227.5-332.4), 194.2± 42.1 MBq (range 141.8-264.5) for ^{68}Ga-FAPI-46, and 195.0±43.1 MBq (range 143.7-272.4) for ^{68}Ga-FAP-2286, respectively. Data were acquired using a hybrid PET/CT (Discovery MI, GE Healthcare) after 1 h of intravenous administration. A low-dose CT scan (100-120 keV; 80-120mA; slice thickness, 3 mm) was collected for attenuation correction and image fusion. All PET images were acquired in 3D mode and were reconstructed by the Bayesian penalized likelihood (BPL) reconstruction algorithm (Q.clear, GE Healthcare).

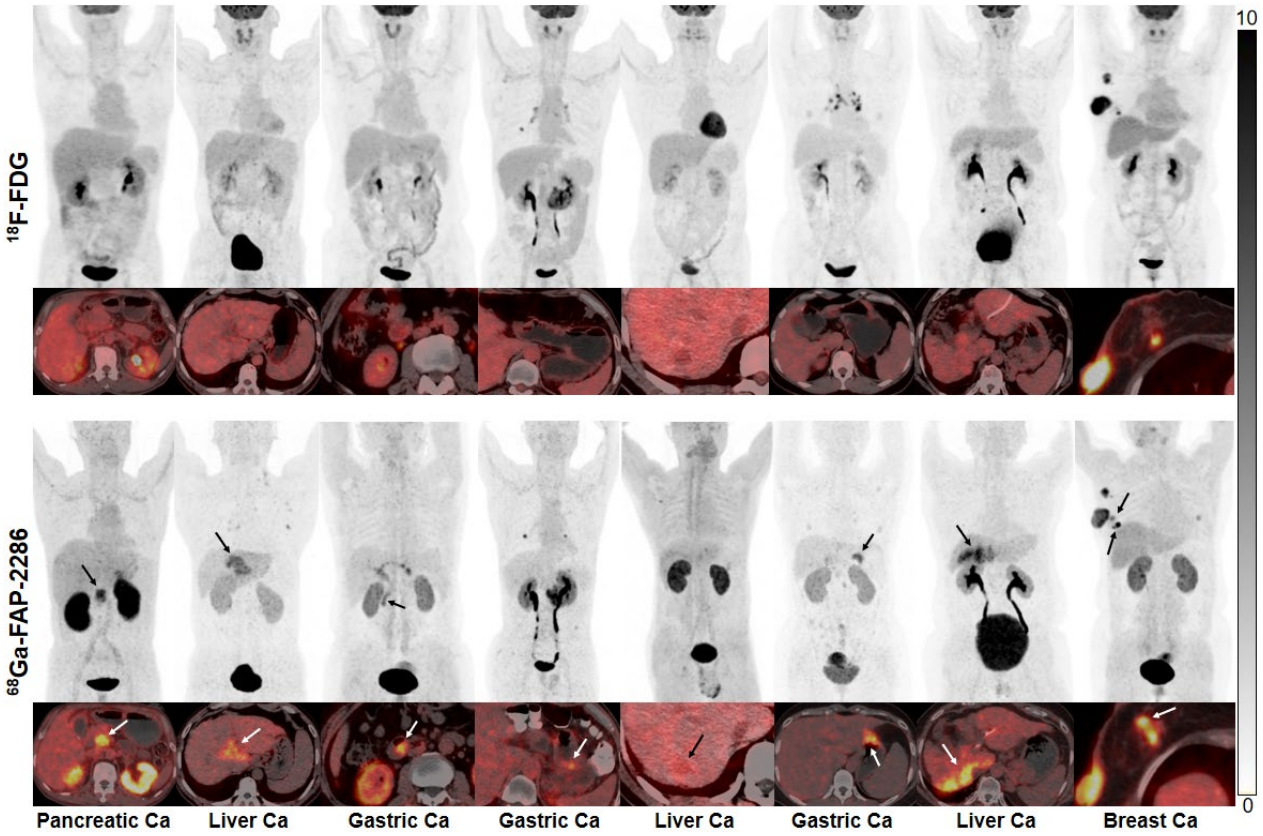

Supplemental Fig. 1 Among the 44 patients underwent PET/CT for initial staging, nine primary tumor lesions from 8 patients were not visualized on ^{18}F-FDG PET/CT, but were well visualized on ^{68}Ga-FAP-2286 PET/CT. The specific tumor entities include gastric cancer (n=3), liver cancer (n=3), breast cancer (n=2), and pancreatic cancer (n=1).

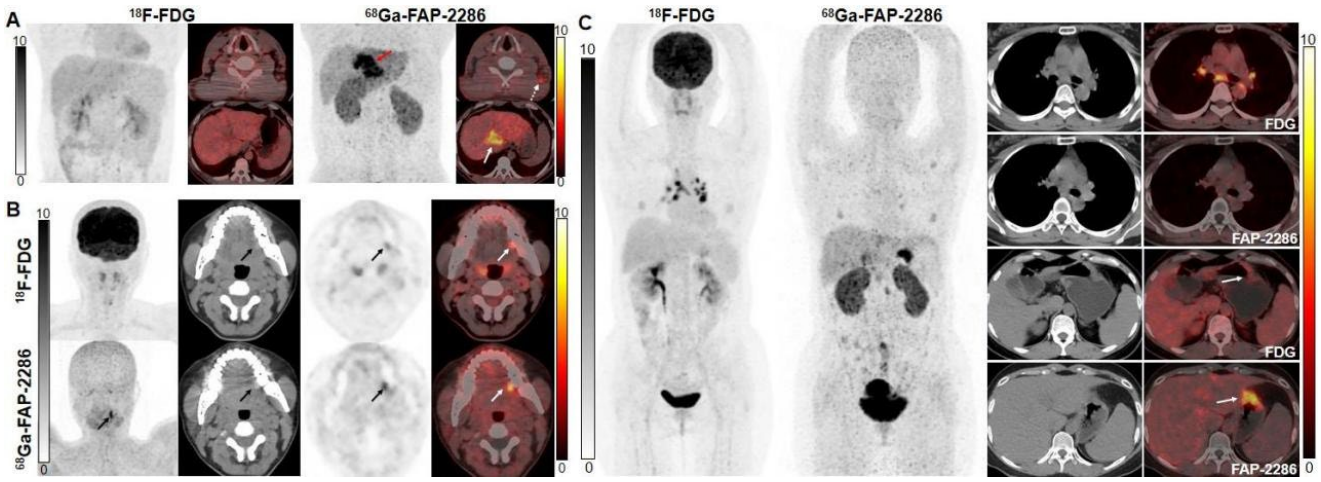

Supplemental Fig. 2 Representative images of patients who underwent ^{18}F-FDG and ^{68}Ga-FAP-2286 PET/CT imaging. (A) A 47-year-old man with known hilar cholangiocarcinoma underwent PET/CT imaging for tumor staging. ^{68}Ga-FAP-2286 demonstrated high tracer uptakes in the primary tumor (solid arrows) and metastatic cervical lymph nodes (confirmed via biopsy, dotted arrows), while ^{18}F-FDG demonstrated no uptake. (B) A 47-year-old woman with tongue cancer who underwent surgical resection, underwent PET/CT imaging after 6 months for the detection of tumor recurrence. Compared to ^{18}F-FDG, ^{68}Ga-FAP-2286 demonstrated a higher tracer uptake in the recurrent tumor lesions (solid arrow). (C) A 40-year-old woman with known gastric signet ring cell carcinoma underwent PET/CT imaging for initial staging. ^{68}Ga-FAP-2286 demonstrated a higher tracer uptake in the primary tumor than did ^{18}F-FDG (solid arrows). Notably, high metabolic activity of the mediastinal lymph nodes was observed for ^{18}F-FDG, while ^{68}Ga-FAP-2286 demonstrated no abnormal activity. The patient subsequently underwent an endoscopic ultrasound fine-needle biopsy, and the pathological results revealed inflammatory lymph nodes.

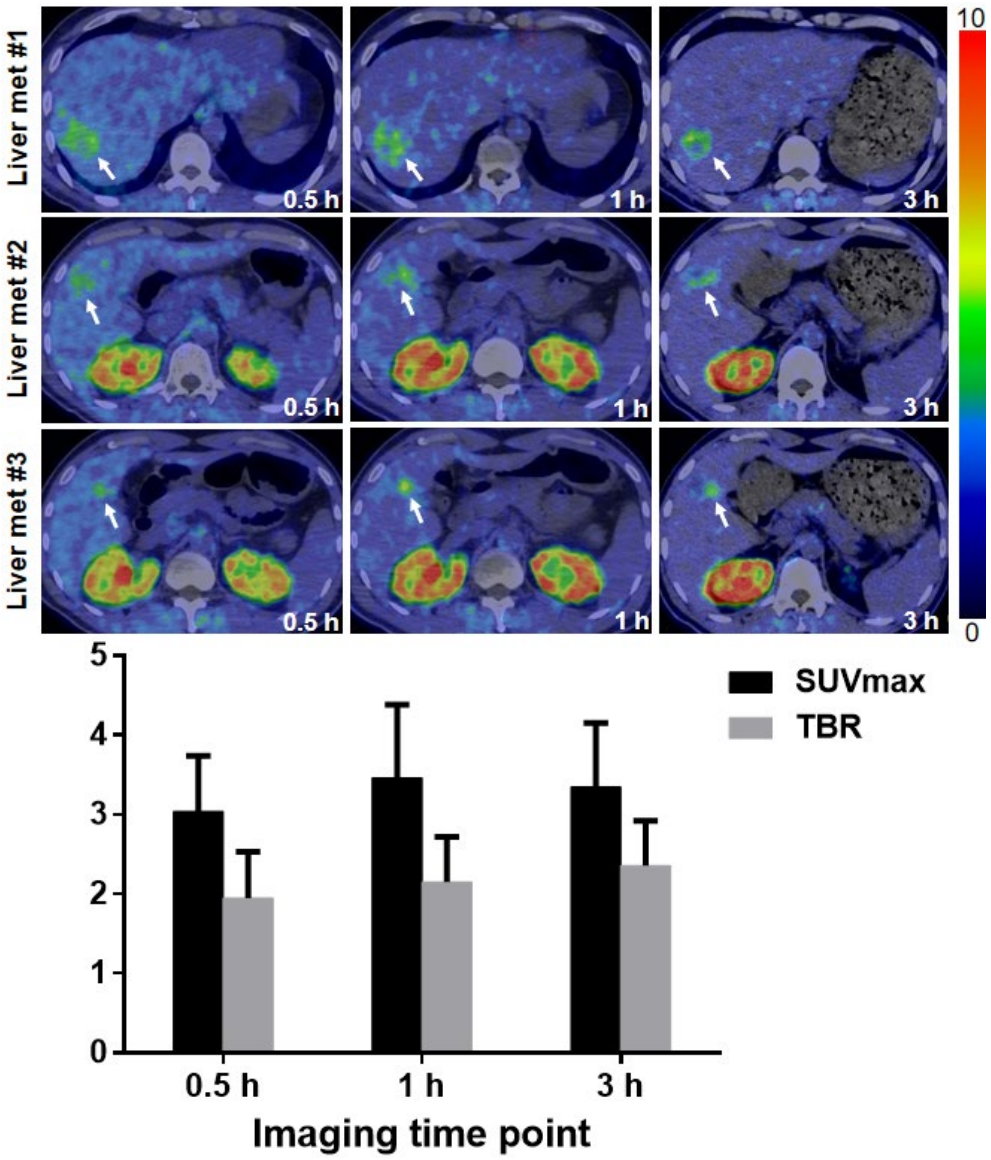

Supplemental Fig. 3 A 40-year-old man with a history of radical resection for colon cancer underwent ^{68}Ga-FAP-2286 PET/CT imaging at different time points after injection. Rapid and stable radiotracer uptake was observed in the liver metastases. Semiquantitative analysis of the liver metastases demonstrated a stable ^{68}Ga-FAP-2286 uptake but an increase in TBR from 0.5 to 3 h.

Abbreviation: FAP = fibroblast activation protein; Met = metastasis; TBR = tumor-to-background ratio.

Supplemental Table 1. Comparison of ^{18}F-FDG and ^{68}Ga-FAP-2286 PET/CT-based TNM staging and recurrence detection in patients with additional findings

Initial Staging

No.	Types of cancer	TNM Stage (FDG-based)	TNM Stage (FAP-2286-based)	Additional finding on FAP-2286 PET/CT (compared to FDG)	Staging change (compared to FDG)
Patient 2	Pancreatic Ca	IIA	IIA	Primary tumor detected	None
Patient 9	Liver Ca (ICC)	IIIA	IIIA	Primary tumor detected	None
Patient 12	Ovarian Ca	IVB	IVB	Larger disease extent of PM	None
Patient 13	HNC (NPC)	IVA	IVB	Bone mets	**Upstaged**
Patient 19	Gastric Ca	IV	IV	Primary tumor detected	None
Patient 21	Pancreatic Ca	IV	IV	More bone mets	None
Patient 25	Liver Ca (HCC)	II	II	Primary tumor detected; More liver mets	None
Patient 27	Pancreatic Ca	III	III	More abdominal LN mets	None
Patient 30	Liver Ca (HCC)	IVB	IVB	More abdominal LN mets and bone mets	None
Patient 31	Pancreatic Ca	IV	IV	Larger disease extent of PM	None
Patient 38	Esophageal Ca	IIIA	IIIB	Greater number of mediastinal LN mets	**Upstaged**
Patient 40	Breast Ca	IIIB	IIIB	More primary tumor detected	None
Patient 48	Gastric Ca	IIA	IIA	Primary tumor detected	None
Patient 49	Gastric Ca	IIA	IIB	Primary tumor detected; More abdominal LN mets	**Upstaged**
Patient 51	Liver Ca (ICC)	II	II	Primary tumor detected	None
Patient 62	Ovarian Ca	IVB	IVB	Larger disease extent of PM	None
Patient 63	HNC (NPC)	IVB	IVB	More bone mets	None
Patient 64	Pancreatic Ca	III	III	More abdominal LN mets	None

Recurrence detection

		Local recurrence detection		Distant metastases detection		Additional finding on FAP-2286 PET/CT
No.	Types of cancer	FDG	FAP-2286	FDG	FAP-2286	
Patient 1	Glioblastoma	-	+	NA	NA	Local recurrence detected by FAP-2286 PET/CT
Patient 11	Gastric Ca	NA	NA	**-**	+	Abdominal LN mets detected by FAP-2286 PET/CT
Patient 22	Liver Ca (ICC)	-	+	**+**	+	Local recurrence detected by FAP-2286 PET/CT; More abdominal LN mets, subcutaneous mets, and bone mets detected by FAP-2286 PET/CT
Patient 24	Liver Ca (HCC)	-	+	NA	NA	Local recurrence detected by FAP-2286 PET/CT
Patient 28	Rectal Ca	NA	NA	**+**	+	Larger disease extent of PM detected by FAP-2286 PET/CT
Patient 34	Liver Ca (HCC)	NA	NA	**-**	+	Liver mets detected by FAP-2286 PET/CT
Patient 36	Gastric Ca	NA	NA	**+**	+	More bone mets and larger disease extent of PM detected by FAP-2286 PET/CT
Patient 43	HNC (Tongue Ca)	-	+	NA	NA	Local recurrence detected by FAP-2286 PET/CT
Patient 46	Renal Ca	NA	NA	**+**	+	More bone mets detected by FAP-2286 PET/CT
Patient 57	HNC (Tongue Ca)	+	+	**-**	+	Muscle mets and liver mets detected by FAP-2286 PET/CT
Patient 58	HNC (Tongue Ca)	-	+	NA	NA	Local recurrence detected by FAP-2286 PET/CT
Patient 59	Liver Ca (HCC)	-	+	NA	NA	Local recurrence detected by FAP-2286 PET/CT

Note. The clinical stage was assigned based on American Joint Committee on Cancer (AJCC) staging system (Eighth edition).

Abbreviations: Ca = cancer, ICC = intrahepatic cholangiocarcinoma, HNC = head and neck cancer, NPC = nasopharyngeal carcinoma, LN = lymph nodes, PM = peritoneal metastases, mets = metastases, HCC = hepatocellular carcinoma, NA = not applicable.